Cement and Concrete Research 41 (2011) 210–216

Contents lists available at ScienceDirect

Cement and Concrete Research

journal homepage: http://ees.elsevier.com/CEMCON/default.asp

The effect of silica availability on the mechanism of geopolymerisation

Ailar Hajimohammadi [a], John L. Provis [a,*], Jannie S.J. van Deventer [a,b]

[a] Department of Chemical and Biomolecular Engineering, University of Melbourne, Victoria 3010, Australia
[b] Zeobond Pty Ltd, P.O. Box 210, Somerton, Victoria 3062, Australia

ARTICLE INFO

Article history:
Received 6 December 2010
Accepted 2 February 2011

Keywords:
Alkali activated cement (D)
Kinetics (A)
Reaction (A)
Nucleation
Characterization (B)

ABSTRACT

The effect of silica availability on geopolymer binder formation is investigated in the geothermal silica–sodium aluminate–water system, using sodium silicate solution as an additional, highly available silica source. Time-resolved and spatially-resolved FTIR data are combined to provide a mechanistic understanding of the role of silica availability in controlling geopolymer nucleation and gel growth behaviour. A higher degree of alumina contribution to geopolymer gels and newly formed crystal phases is observed in systems with higher silica availability. Gel nucleation is observed to take place in the region immediately surrounding the solid silica source particles when no dissolved silica is initially supplied. Conversely, mixes which initially contain dissolved silica show nucleation in bulk regions, and involving more of the Al which is rapidly released from the sodium aluminate precursor. These differences in nucleation lead to a more chemically heterogeneous binder in the case where silica is released more gradually.

1. Introduction

Geopolymer binders, formed by alkaline activation of aluminosilicate precursors, are attracting interest as a "green" cement [1–3], because through the use of industrial wastes such as geothermal silicas, fly ashes and mineralogical slags as source materials, there is the possibility to achieve a significantly lower CO_2 emission per tonne in comparison with OPC [1,2,4,5]. With increasing production volumes, geopolymer and other alkali-activated binders are also becoming cost-competitive with Portland cement, and have found utilisation in major infrastructure projects internationally; initially in the former Soviet Union and in China [6–8], and now increasingly in Australia and elsewhere internationally as the political and financial incentives for CO_2 emission reductions grow [3].

However, there are many aspects of geopolymer synthesis chemistry which are not yet fully understood. There has been detailed analysis of the roles played in the geopolymer synthesis process by the kinetics of availability of alumina [9–12] and calcium [13,14] within geopolymer-forming systems, and the effect of silica concentration is well known [15–19], but little has been published regarding the effect of the rate of silica release in determining geopolymer gel structure and reaction mechanisms. This is mainly due to the difficulty associated with separating the effects of silica availability (in terms of reaction kinetics) and silica concentration within the limitations of a standard 'two-part' (solid precursor plus alkaline activating solution) geopolymer mix.

Sodium aluminate solution and silica fume have previously been used to make simplified 'two-part' geopolymer mixtures [20], and the recent development of 'one-part' (solid precursor plus water) geopolymer mixes based on very finely divided silica (silica fume or geothermal silica) and solid sodium aluminate [21,22] provides opportunities for advances in this area. It is now possible to design geopolymer mixes with the same composition and alumina release rates, while tailoring the silica release rate by using either sodium silicate solution, geothermal silica, or a mixture of the two. This provides the opportunity to directly control silica release rates, and to study geopolymer chemistry and performance as a function of silica availability in the initial stages of the reaction.

From the information available to date, it is believed that high early silica availability should lead to faster conversion of solid aluminosilicate sources to geopolymer gel [23,24]. However, it is not known whether this more rapid conversion (which can also be achieved to some extent by nanoparticle seeding of the reaction mixture [25,26]) is specifically desirable in terms of microstructure and strength development. Thus, understanding geopolymer characteristics as a function of the rate of silica availability will be important in understanding and controlling the behaviour of geopolymeric binders.

Analysis of geopolymers using synchrotron radiation-based Fourier transform infrared (SR-FTIR) spectromicroscopy has shown the capabilities of this powerful technique in spatially-resolved investigation of chemical variations in geopolymeric binders [11]. This paper presents the results of an investigation using this technique, along with X-ray diffraction and time-resolved FTIR spectroscopy, to analyse the effects of timed release of silica on the nanostructure and microstructure of geopolymer binders. Sodium aluminate is the

* Corresponding author. Tel.: +61 3 8344 8755; fax: +61 3 8344 4153.
E-mail address: jprovis@unimelb.edu.au (J.L. Provis).

0008-8846/$ – see front matter © 2011 Elsevier Ltd. All rights reserved.
doi:10.1016/j.cemconres.2011.02.001

alumina source for all samples produced here; geothermal silica is used as a 'slow release' silica source, and waterglass (sodium silicate solution) where more rapid silica availability is desired.

2. Materials and methods

To synthesise a geopolymer mix with relatively slow silica availability (denoted G1), washed, dried and milled geothermal silica (Cerro Prieto geothermal power station, Mexico, 96 wt.% SiO_2, loss on ignition 1.3 wt.%, remainder <0.5 wt.% of each of Na, Mg, Al, K, Ca, Mn and Fe [22]) was mixed with solid sodium aluminate (Aldrich; 55.2 wt.% Al_2O_3 and 42.7 wt.% Na_2O) to attain an SiO_2/Al_2O_3 molar ratio of 3.0:1, and then water was added to this solid mixture to give an H_2O/Na_2O molar ratio of 7.0:1 (i.e. overall $Na_2O/Al_2O_3 \approx 1.3$).

To provide more rapidly available silica, a commercial sodium silicate solution (Grade N, PQ Australia), with composition 8.9 wt.% Na_2O, 28.7 wt.% SiO_2 and 62.4 wt.% H_2O, was also used. Two mixes (denoted G2 and G3) were made with the addition of this silicate solution; a summary of the compositions of the three samples is presented in Table 1. In G2, the Si source blend was 85 wt.% from geothermal silica and 15 wt.% from sodium silicate solution (giving overall $Na_2O/Al_2O_3 \approx 1.4$), while in G3, the Si source was 70 wt.% from geothermal silica and 30 wt.% from sodium silicate solution (giving overall $Na_2O/Al_2O_3 \approx 1.5$). As the difference in Na_2O/Al_2O_3 ratios across the sample set was less than 0.2, NaOH was not added to adjust the composition for these samples. Sodium aluminate was also used in samples G2 and G3 as the sole alumina source, as well as providing alkali, and the raw material composition was adjusted to maintain similar SiO_2/Al_2O_3 and H_2O/Na_2O molar ratios of 3.0:1 and 7.0:1 respectively. Therefore, three mixes were made with different silica availabilities but similar compositions, with G3 having the highest silica availability in the early stages of the reaction and G1 having the lowest silica availability. All samples were sealed and cured at 40 °C until analysis.

Crystalline phases were identified using X-ray diffraction (XRD) (Phillips PW-1800) with CuKα X-rays, operating at 30 mA and 40 kV with 0.02° 2θ steps, 2 s $step^{-1}$. Structural characteristics of geopolymeric binders were also studied using attenuated total reflectance Fourier-transform infrared (ATR-FTIR) spectroscopy. ATR-FTIR spectra were collected using a Varian FTS 7000 spectrometer, with a Specac MKII Golden Gate single reflectance diamond ATR attachment with KRS-5 lenses. Absorbance spectra were collected from 4000 to 400 cm^{-1} at a resolution of 2 cm^{-1} and a scanning speed of 5 kHz, with 32 scans/spectrum.

Synchrotron FTIR spectromicroscopy (SR-FTIR) was used to investigate the structural heterogeneity of geopolymer samples, using the microscopy endstation on BL8 (Infrared Spectroscopy) at the Australian Synchrotron, Melbourne. Sample preparation included cutting with a diamond saw, then polishing with increasing fineness up to 6 μm diamond paste, using the same polishing technique as applied previously for the study of geopolymers by electron microscopy [27]. By using the optical microscope attached to the FTIR microscopy endstation, regions of interest were defined on each sample as rectangles 30×20 points in size, on a 10 μm grid spacing. A 20×20 μm aperture size was used. After defining the positions, FTIR data were collected at each point using an ATR crystal, 64 scans/spot, from 3000 to 700 cm^{-1}.

Table 1
Molar ratios of the components of the three samples used in this paper.

Sample	SiO_2/Al_2O_3	Na_2O/SiO_2	H_2O/Na_2O
G1	3.0	0.43	7.0
G2	3.0	0.46	7.0
G3	3.0	0.50	7.0

The hierarchical clustering analysis (HCA) method was applied to the analysis of SR-FTIR data using the CytoSpec software package. Baselines were corrected across the full spectra, then the region from 800 to 1200 cm^{-1} in each spectrum was normalised using the Vector normalisation method. Finally, smoothing was applied using the average smoothing algorithm as implemented in the Cytospec software.

3. Results and discussion

3.1. Characterising crystalline phases

Fig. 1 shows the XRD data obtained for three geopolymer samples with different silicon availabilities after different curing times. Crystalline phases identified include quartz (SiO_2; Powder Diffraction File (PDF) card: 00-046-1045), sodium metasilicate ($Na_2SiO_3 \cdot 9H_2O$; PDF: 00-019-1239), sodium silicate (Na_4SiO_4; PDF: 00-032-1154), zeolite A (approximately $Na_2Al_2Si_{1.85}O_{7.7} \cdot 5.1H2O$; PDF: 00-038-0241), faujasite (approximately $Na_2Al_2Si_4O_{12} \cdot 8H_2O$; PDF: 00-039-1380), analcime (approximately $Na_{3.6}Al_{3.6}Si_{12.4}O_{32} \cdot 14H_2O$; PDF: 00-044-0052) and natrite (Na_2CO_3; PDF: 00-037-0451). The formation of carbonates is attributed to improper sealing of the samples, which allows atmospheric CO_2 to react with the sodium-rich pore solutions. As the intensity and sharpness of the carbonate peaks in the XRD results did not change over time, and no obvious difference was observed at 1400 cm^{-1} (which is a sensitive and well-defined band related to C–O vibrations in carbonates [28]) in the FTIR spectra of the three samples, the differences in the extent of carbonation between samples do not appear significant.

Quartz, which is recognisable in all samples after two days (Fig. 1a), is the main crystalline phase present in geothermal silica, and the sodium silicate phases which are formed in the early stages of the reaction in samples G2 and G3 are absent in G1. After four days (Fig. 1b), zeolite A is the main crystal phase recognisable in G1, while in G2 and G3 there are also some peaks related to faujasite. In 21 days, G1 has also developed the faujasite phase, and the XRD data for all samples after three weeks look reasonably similar to each other, although differing in the relative concentrations of the zeolitic phases (faujasite and zeolite A). This indicates that similar chemical changes are taking place in all samples, but with different rates. Sample G1, with the lowest Si availability, was the sample which took the longest to develop the zeolitic phases. Sample G2 shows the highest extent of crystallite formation, and the sharpest zeolite diffraction peaks, while G3 shows less faujasite than G2.

There are two main differences between G1 and the other two samples, after 21 days (Fig. 1c). One is the formation of a considerable amount of analcime in G1, which is a very minor phase in G2 and G3, and the other is the absence of the sodium silicate phase which is formed in the other two samples. Analcime is a relatively high-silica crystalline phase, and the formation of higher amounts of this phase indicates that there has most likely been a high-silica environment in the regions of the gel in which it formed, as has been discussed previously for geopolymer-forming systems [11] and for zeolite synthesis by hydrothermal transformation of gels and clays [29].

The formation of analcime in G1 is somewhat unexpected, as samples G2 and G3 have higher silica availability than G1, meaning that the formation of silica-rich crystals could be expected in these samples rather than G1. The fact that this was not observed may be due to the heterogeneity of the samples, leading to the growth of different phases in local areas, or also it could be a sign of a higher degree of Si contribution to the final geopolymer binder due to the favourable activating energy of the transformation of such regions (compared to less Si-rich regions) to higher-Si crystallites, as has been explained in detail elsewhere [11].

The formation of identifiable sodium silicate phases in G2 and G3 is also relatively unusual in geopolymer-forming systems, and indicates

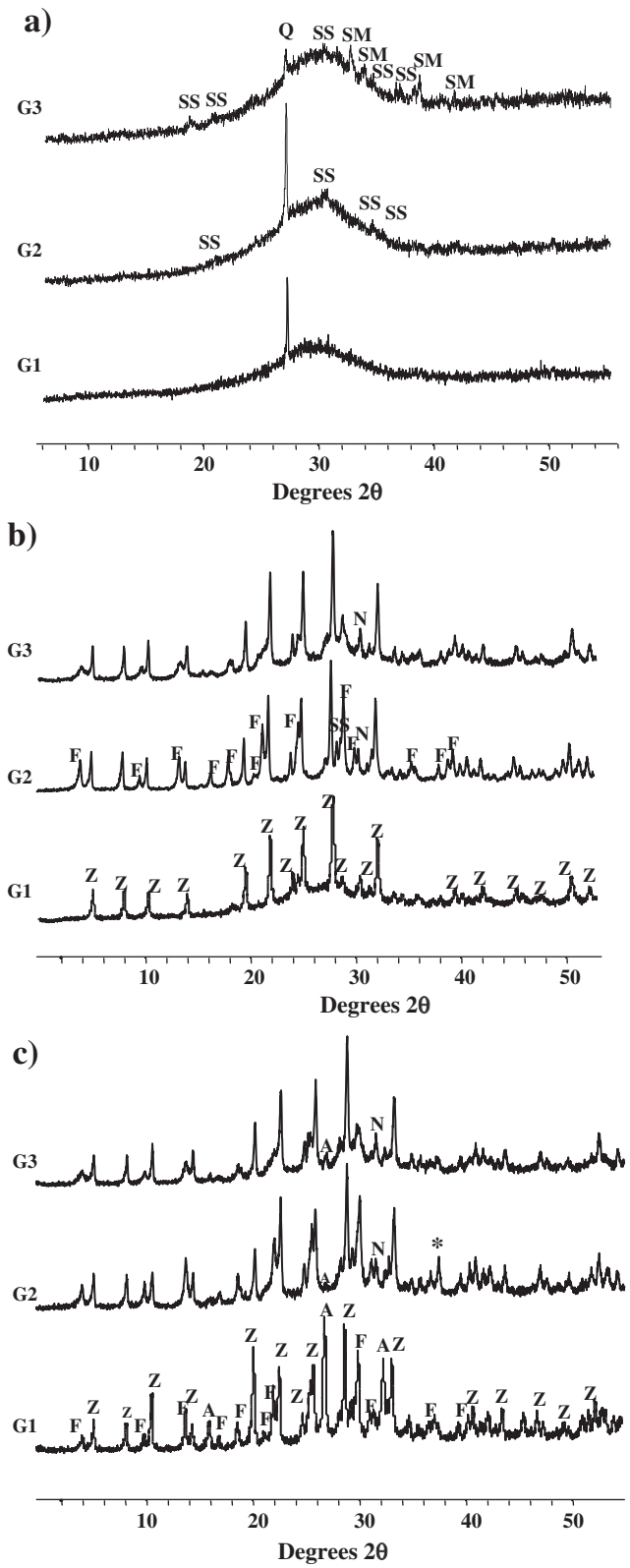

Fig. 1. Cu Kα X-ray diffractograms of geopolymer samples G1, G2, and G3 (as labelled) after: a) 2 days, b) 4 days and c) 21 days of curing at 40 °C. Q: quartz, SM: sodium metasilicate, SS: sodium silicate, Z: zeolite A, F: faujasite, A: analcime. The peak marked with * is aluminium from the sample holder. Where peaks in G2 and G3 are not labelled, these correspond to the same phases as marked in G1.

that some of the initially dissolved silica has precipitated, along with alkali cations, during the initial period of reaction. The relatively dilute (by the standards of geopolymer activating solutions) sodium silicate-containing aqueous phase was initially kinetically stable with respect to precipitation [30], but inspection of the phase diagram for this system [31] shows that the release of alkalis from the sodium aluminate may have destabilised the solution and led to the observed precipitation. It is rare in the literature for a geopolymer-forming mix to contain a significant quantity of alkalis contributed by the solid reactants when an alkali silicate activator is used, which is possibly why this destabilisation and precipitation is not often observed. It also appears that the role played by Al in directing gel formation in this system does not prevent the behaviour predicted from the Na_2O-SiO_2-H_2O ternary system from being observed, at least in part.

3.2. Nanostructural analysis

Fig. 2 shows the changes in the ATR-FTIR spectra of the three mixes as a function of curing time. As observed previously for similar geothermal silica-sodium aluminate systems [22], the intensity of the peak related to unreacted silica (1060 cm^{-1}) decreases as the reaction proceeds, and a new peak forms at about 960 cm^{-1} which is related to the stretching vibrations of Si–O–Si and Si–O–Al in newly formed geopolymer gels.

As there is dissolved silica present in the raw materials for samples G2 and G3, the zero time spectra of these samples (obtained immediately after mixing) differ from that of G1, showing the contribution of dissolved silicate species. The increased intensity in the region between 900–1000 cm^{-1} in these spectra compared to G1 at zero time can be related to Si–OH vibrations in solvated structures [32]. Once the geopolymer network begins to grow, the peak close to 960 cm^{-1} (which overlaps with some of the dissolved species contribution) again begins to grow, and can be assigned to the asymmetric stretching vibrations involving Si–O–T (T: Si or Al) and/or non-bridging oxygen sites in a silicate network [22,24,33]. As the alkalinities of all samples are similar, significant differences in the extent of non-bridging oxygen formation are improbable, and so the bands at about 960 cm^{-1} in samples G2 and G3 will be related to both Si–OH bonds and the newly formed Si–O–T network, but differences between the samples in this region are attributed to the Si–O–T network rather than differences in Si–OH site formation. Table 2 shows the IR band assignments for the main spectral region studied in this paper.

As geothermal silica has a high surface area and dissolves relatively quickly, after two days the FTIR spectra of all samples in Fig. 2 look very similar. However, one apparent difference between the spectra is the breadth of the "main band" (the strong peak in the Si–O–T asymmetric stretch region) in G1. This might be because of a higher degree of heterogeneity in this sample and thus the existence of a broader range of different structural features; the main band in geopolymer samples is always a composite of many peaks, and although deconvolutions of this type of featureless peak for geopolymers have been attempted in the past [36], such an approach does not appear to provide useful results here due to the lack of *a priori* information from which to determine peak positions and widths for use in the deconvolution process. Because of this, and because ATR-FTIR as applied here does not provide lateral spatial resolution across a sample surface, no direct comment can be made regarding the degree of heterogeneity present based purely on these results. However, this point will be addressed more specifically in the following section by the application of SR-FTIR.

Another key difference between the samples is the final position of the main band. Upon increasing silica availability in samples G2 and G3, the position of the main band shifts to lower wavenumbers, which is contrary to previous findings regarding the effect of soluble silicates on the FTIR spectra of fly ash geopolymers [21]. Fig. 3 summarises the observed behaviour, presenting the changes in peak position with time for the three samples. As was expected from observations of fly ash systems activated by silicate solutions [37], the final main band

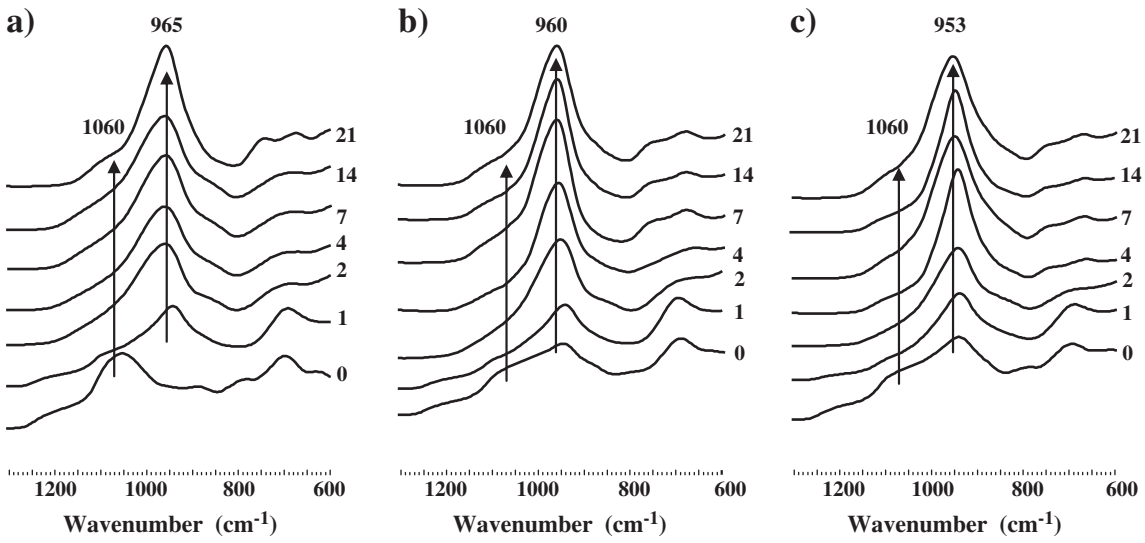

Fig. 2. Evolution of ATR-FTIR spectra for samples a) G1, b) G2 and c) G3 over time. Key peak positions are marked, and the numbers alongside the spectra refer to the ages of samples in days.

position in each of samples G2 and G3 is close to the minimum peak position observed for these mixes, and neither of these two samples shows a large peak shift in the early stages of the reaction. The time at which the minimum in peak position occurs is similar for all three samples, suggesting that formation of Al-rich gel followed by Si-rich gel [9] takes place at around the same rate for all samples, but with different Si/Al ratios in the developing gels as shown by the different minimum peak positions.

The fact that the lowest peak position was observed for G3, followed by G2 and G1, indicates that more Al participates in the geopolymer gel structure when there is higher Si availability in the mix. Although this correlates well with the formation of a considerable amount of analcime as a crystalline phase in sample G1, it was unexpected because, based on the existing understanding of traditional geopolymer-forming systems [9,38], higher Si contribution to geopolymer gels would be expected when a higher amount of soluble silicates was available in the early stages of the reaction.

It is known from previous work using fly ash-derived geopolymer systems [11] that, when alumina was more readily available in the early stages of reaction, the initially-formed geopolymer gel contained a high level of Al, and its main band shifted to lower wavenumbers than in comparable samples with slower alumina release rates. When enough silica was then released from the solid precursors used, and become incorporated into the gel structure, the main band shifted back to higher wavenumbers. Conversely, when there was slower release of alumina and relatively more silica participation in the initial "Al-rich" gel, this initial gel was more stable than the very Al-rich phase formed in the rapid Al-release sample, and so showed less variation in peak position in the time after the minimum was observed [11]. These observations may be used in part to guide the discussion here regarding Si release rates, which could be expected to be to some extent analogous. However, to provide an explanation for why there is a lower apparent Si/Al ratio in sample G3 here, while there is similar Al availability in all samples and more Si readily available for reaction in G2 and G3 than in G1, requires more information regarding the local chemistry of these geopolymer gels. The key question is why the higher availability of alumina in solution leads to greater participation of Al in the gel structure in the early stages of geopolymerisation, while the same higher extent of Al participation is also observed with higher availability of Si.

The main difference between the fly ash geopolymer systems studied previously [11] and the samples analysed here is the nature of the source that supplies Si and Al to the system. In fly ash geopolymer systems, fly ash particles are a key source of both the Si and the Al needed for reaction, and the silica dissolution rate from fly ash is interlinked with the dissolution rate of alumina [25,39]; dissolution is not necessarily congruent, but the local structural degradation of the ash particles caused by the release of one of the components will accelerate the removal of the other. Additionally, in those systems, the newly dissolved species of Al and Si are both released into the solution region immediately surrounding the ash particles, and can react there to form geopolymer gel [40]. Conversely, in the geothermal silica-sodium aluminate geopolymers studied here, the Al and Si sources are distinct from each other, and the dissolution rate of sodium aluminate is very high, meaning that dissolved Al species will be readily available in solution, while the dissolution of geothermal silica is somewhat slower (although still faster than fly ash), and will also depend on the local concentration gradient of silica. This will be expected to introduce some differences in the local chemistry of geopolymer gels forming in these two types of systems.

Table 2
Characteristic IR vibration bands of interest.

Wavenumber (cm^{-1})	Assignment	References
850	OH bending (Si–OH)	[34]
900–1000	Non bridging oxygen (Si–O), asymmetric stretch Si–O–(Si, Al)	[22,24,33]
1060	Stretching vibration- surface Si–O–Si	[35]
1090–1100	Stretching vibration-bulk Si–O–Si	[21]

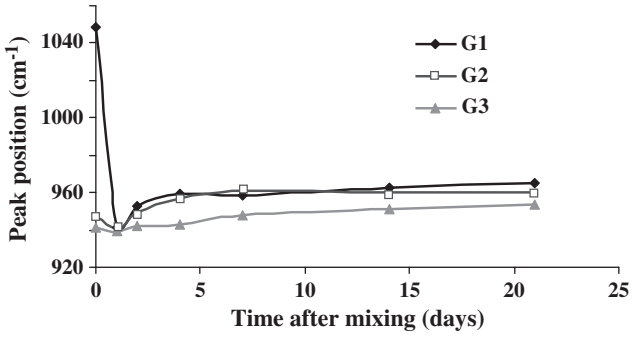

Fig. 3. Variation in main Si–O–T peak position with sample age.

Nucleation is also known to play a key role in the mechanism of geopolymer gel formation [18,25,41]. The sites where nuclei form are where the formation of geopolymer gel begins, and therefore the local composition of the reacting systems in these places can affect the extent of participation of nutrients in geopolymer gels. Thus, it can be hypothesised that the higher contribution of Al to the gels in samples G2 and G3 is related to the locations where nucleation first occurs in these samples. While the availability of Al is similar in all samples, there is a difference in Si availability in the three samples. In G1, the only Si source is geothermal silica, and therefore enough Si must dissolve and react with Al to generate a stable nucleus for further gel growth, while in G2 and G3, there is soluble Si immediately available to react with Al and form the required nucleus in solution. Therefore, nucleation in sample G1 is able to occur closer to the silica particles where there is enough dissolved Si available to react with the dissolved Al existing in the surrounding environment, whereas in G2 and G3 nucleation will be more likely to occur first in solution or closer to aluminate particles, where enough soluble Al is available to react with the available dissolved silica.

This spatial difference in nucleation can cause two main mechanistic differences between the samples with and without added soluble silicates. One is the formation and growth of geopolymer gels mainly in areas relatively rich in Si in G1, but in areas rich in Al in G2 and G3. The other is the generation of different concentration gradients of Si, and therefore different driving forces for silica dissolution. There will be a greater driving force for silica dissolution in samples G2 and G3, in which the initial gel formation takes place further from the unreacted silica particles, and consequently a higher extent of dissolution of silica particles would be expected in these samples. If this heterogeneity is in fact responsible for the different levels of Al and Si contributions in these geopolymer gels, and influences the extent of dissolution of unreacted silica, the application of SR-FTIR will be valuable in studying the differences in the degree of heterogeneity between the samples.

3.3. Spatially-resolved infrared spectroscopy

Fig. 4 presents the results of SR-FTIR microscopy as applied to samples G1 and G2; these two mixes were selected for analysis by SR-FTIR because scanning electron microscopy [26] showed the microstructure of G3 to be very porous and thus not well suited to the polishing required for SR-FTIR analysis. In these 'chemical map' plots, the wavenumber of the main FTIR band is colour coded and plotted versus the spatial x–y coordinates. Wavenumbers of 920 cm^{-1} and 1000 cm^{-1} were used as the lower and upper bounds of the spectral region analysed, to isolate features due to geopolymer gels. In a chemical map, the presence of more areas with similar colours means that the positions of the main FTIR bands in the spectra obtained at each point are more uniform, indicating the formation of more homogeneous geopolymer gels. Conversely, the presence of regions with very different colours indicates a higher degree of heterogeneity. Therefore, sample G2, which shows greater uniformity in main band position (Fig. 4b), is characterised on this length scale as being a more chemically homogenous sample. This also aids in confirming that the broader peaks in the ATR-FTIR analysis of sample G1 (Fig. 2) were in fact related to a higher degree of heterogeneity in this sample.

The results of hierarchical clustering (HCA) analysis [11] applied to the SR-FTIR data for samples G1 and G2 are presented in Fig. 5. Four different spectral clusters could be identified for each sample; clustering is achieved by identifying the two mathematically 'most similar' spectra obtained from different regions on the same sample, labelling these as a 'cluster' represented by the average of the two spectra, and then repeating this procedure iteratively until all spectra obtained for a sample are classified into a small number of distinct clusters. The procedure is carried out independently for each sample. Full details of the algorithm used are given in reference [11]. The regions corresponding to each cluster are colour coded, and the average spectrum representing each cluster is presented in the same colour in Fig. 5.

For sample G1, the HCA results in Fig. 5a show that two similar peaks and a shoulder can be observed in the different clusters. In the dominant spectral clusters (yellow and orange), there is a relatively large shoulder at about 1090 cm^{-1}. Also, two notably different positions for the main Si–O–T bands in the different clusters (945 cm^{-1} in yellow and orange, and 975 cm^{-1} in brown and black) can be identified. In sample G2 (Fig. 5b), there are a small number of yellow regions related to the spectrum with main bands at 1090 cm^{-1} and 952 cm^{-1}, and the 1090 cm^{-1} band more intense than the 952 cm^{-1} band. The remainder of the clusters in sample G2 each contain two main bands: a major band at about 952 cm^{-1} and a less prominent band at about 850 cm^{-1}.

Comparing the spatially resolved and time resolved FTIR data, using the peak assignments presented in Table 2, can then aid in understanding the local chemistry of geopolymer binders. The bands at 1060 cm^{-1} and 1090 cm^{-1} are related to Si–O–Si stretching vibrations of the surface and bulk of unreacted silica particles respectively [21,35]. Thus, in sample G1, the large shoulder at 1090 cm^{-1} in the dominant (yellow) spectrum is related to unreacted

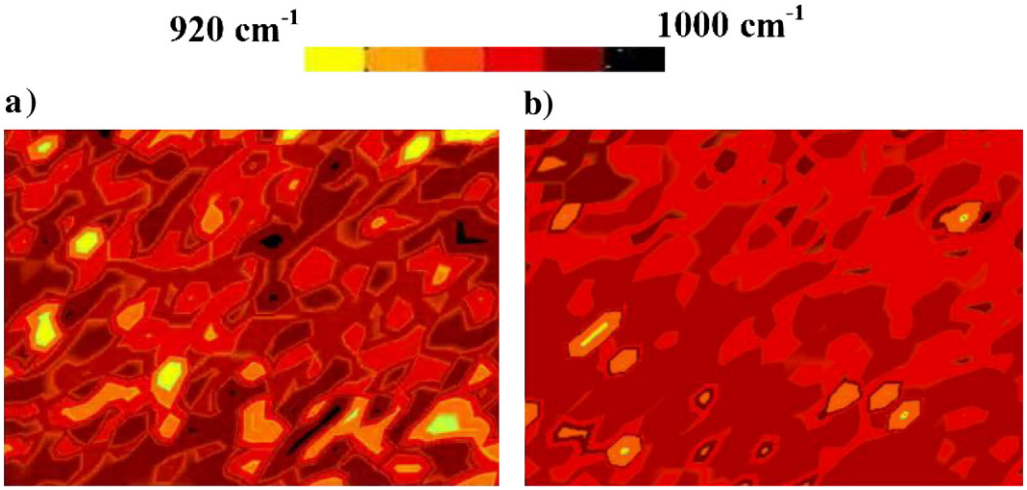

Fig. 4. Peak position maps in the 920 cm^{-1}–1000 cm^{-1} region for samples: a) G1, and b) G2. Black shows areas with the main band position close to 1000 cm^{-1}, and yellow shows regions with the main band position closer to 920 cm^{-1}, as shown in the colour scale above the plots. The region mapped is 300 × 200 μm in each case.

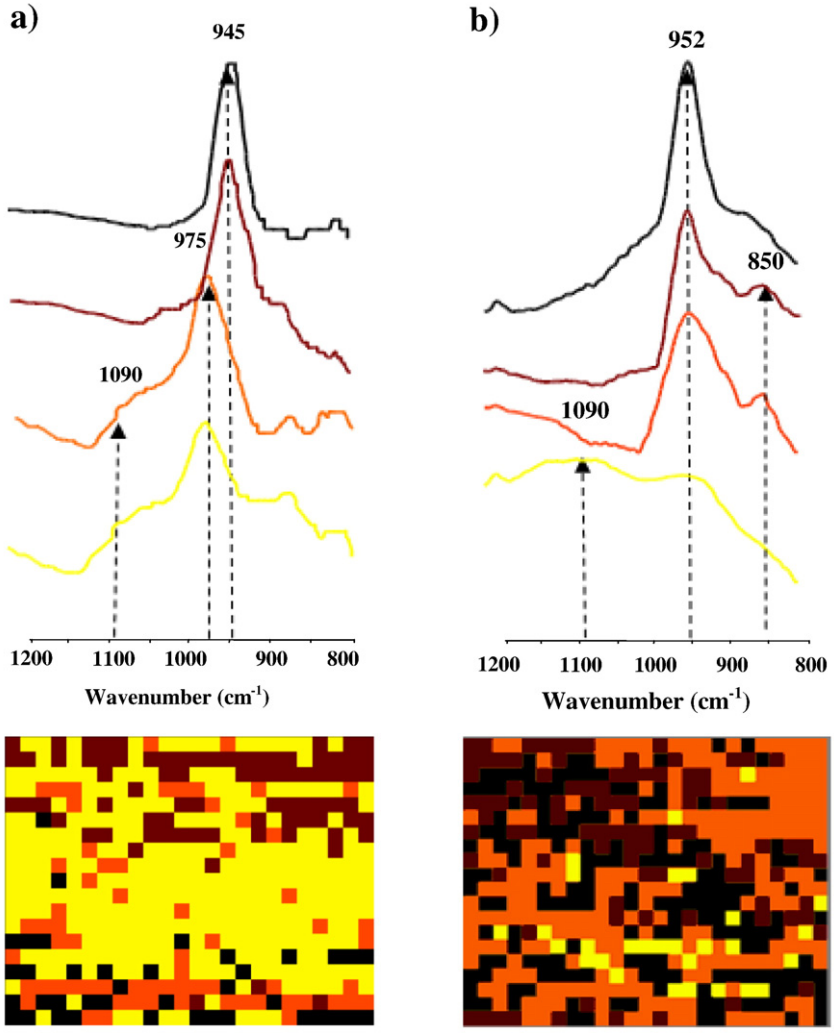

Fig. 5. Spatially resolved FTIR spectromicroscopy (SR-FTIR) data obtained after two months of curing, with hierarchical clustering analysis of a) sample G1 and b) sample G2. The region mapped is 300 × 200 μm in each case.

silica particles, while the dominant (orange) spectrum in G2 has only a very small shoulder at this wavenumber, indicating a higher extent of silica dissolution in this sample.

However, there are a small number of regions in sample G2 which have the main band at 1090 cm^{-1} and a smaller band at 952 cm^{-1}. This spectrum is very similar to the ATR-FTIR spectrum obtained at zero time for this sample (Fig. 2b), indicating that the areas related to this spectrum have mainly remained unreacted. The main bands at 952 cm^{-1}, 945 cm^{-1} and 975 cm^{-1} are related to the presence of newly formed geopolymer gel regions with different Si/Al ratios in their gel networks. The band at 850 cm^{-1} is related to the vibration of Si—OH bonds [34], and the existence of a significant peak at this wavenumber for some regions in both samples indicates the presence of silica species which have not yet fully participated in geopolymerisation after two months of curing.

These spatially-resolved data are also helpful in evaluating the hypothesis presented earlier regarding the spatial differences between nucleation sites in the samples studied here, and the corresponding influence on the heterogeneity of geopolymer gels. In sample G1, the band at 945 cm^{-1} is due to geopolymer gel with a relatively high Al content, and the band at 975 cm^{-1} shows areas where the geopolymer gels are richer in Si. The dominant spectra (yellow and orange) of this sample in Fig. 5a contain geopolymer gels with the main band at 975 cm^{-1} and a relatively strong shoulder at 1090 cm^{-1}. This suggests two things: first, that most of the geopolymer gels formed in this sample are higher in silica content (confirming the observations based on the main band peak positions in Fig. 3), and second, that these geopolymer gels are formed in the areas very close to the unreacted silica particles. The unreacted particles cannot specifically be distinguished from the gel regions at the resolution (>10 μm) of the SR-FTIR instrument used here, but the presence of the 1090 cm^{-1} peak provides evidence of their presence in certain regions. The regions close to the unreacted silica particles were the nucleation sites hypothesised based on the ATR-FTIR data for mix G1, and the SR-FTIR information appears consistent with this proposal. Thus, in G1 with no initially-supplied dissolved silica, nucleation occurs close to the silica particles, where the silica dissolves and becomes available to react with the rapidly-available dissolved Al.

On the other hand, in sample G2 (Fig. 5b), regions with a strong unreacted silica band at 1090 cm^{-1} are very scarce. In the areas where reaction has taken place, the main band is at about 952 cm^{-1}, and there is another band at 850 cm^{-1} related to Si–OH vibrations. These results suggest three important things: first, the main geopolymer gel in this sample is richer in Al and/or less cross-linked (as seen by the lower wavenumber of the main Si–O–T band), which is consistent with the peak position data in Fig. 3. Elemental analysis under scanning electron microscopy [26] shows only a slightly lower Si/Al ratio in the gel of G2 than G1, meaning that some difference in the extent of gel crosslinking is also likely. Second, the newly formed gel is in the regions which were originally occupied by solution, further from unreacted silica particles (as seen by the presence of a significant

850 cm^{-1} band and only a very small shoulder at 1090 cm^{-1} in the main well-reacted areas). Third, although there is more extensive dissolution of silica particles in this sample than in G1, the degree of cross linking to form geopolymer gel is not yet complete even after two months of curing (again indicated by the 850 cm^{-1} band). These findings again support the hypothesis presented above regarding the nucleation sites in G2; nucleation in this sample occurs first in solution or closer to aluminate particles, where enough Al is available to react with the already-dissolved silica. This difference, when compared with the nucleation mechanism of G1, causes different concentration gradients of Si and therefore different driving forces for silica dissolution as a function of silica availability, and shows the tailoring of geopolymer gel structure by reaction kinetic considerations.

4. Conclusions

The effects of the early availability of silica on aluminosilicate geopolymer binder structure have been investigated. A higher-silica crystalline phase, analcime, was identified in the sample with the lowest silica availability, in addition to the zeolites formed in all samples. Time-resolved infrared spectroscopy suggested, somewhat counter-intuitively, that increasing Si availability led to more contribution from Al in the geopolymer network. This was attributed to differences in gel nucleation sites between the samples with and without initially dissolved (rapidly available) silica. When the silica is all supplied in solid form, nucleation takes place closer to unreacted silica particles, as the silica released from the particles first encounters the rapidly-available alumina in those regions. Conversely, for samples with higher silica availability (dissolved silica initially present as an alkaline silicate activating solution), nucleation occurs further from the unreacted silica particles, as the first encounters between silica and alumina are not dependent on the release of silica by dissolution in these samples. Spatially resolved infrared microscopy (SR-FTIR) supported these conclusions regarding nucleation sites, and also showed a higher extent of silica dissolution in these samples. The infrared microscopy data also showed a more homogenous geopolymer gel binder with increasing silica availability, and provided information regarding the local distribution of chemical bonding environments which has not been available from any other analytical technique.

Acknowledgements

This work was funded in part by a studentship provided to Ailar Hajimohammadi by the Centre for Sustainable Resource Processing through the Geopolymer Alliance, and in part by the Australian Research Council (including through the Particulate Fluids Processing Centre). We gratefully acknowledge the assistance of Dr Mark Tobin and Dr Ljiljana Puskar of the Australian Synchrotron. This research was undertaken on the BL8 (Infrared Spectroscopy) beamline at the Australian Synchrotron, Victoria, Australia. The views expressed herein are those of the authors and are not necessarily those of the owner or operator of the Australian Synchrotron.

References

[1] P. Duxson, J.L. Provis, G.C. Lukey, J.S.J. van Deventer, The role of inorganic polymer technology in the development of 'Green concrete', Cem. Concr. Res. 37 (12) (2007) 1590–1597.
[2] J. Davidovits, Geopolymer Chemistry and Applications, Institut Géopolymère, Saint-Quentin, France, 2008.
[3] J.S.J. van Deventer, J.L. Provis, P. Duxson, D.G. Brice, Chemical research and climate change as drivers in the commercial adoption of alkali activated materials, Waste Biomass Valoriz 1 (1) (2010) 145–155.
[4] J.W. Phair, Green chemistry for sustainable cement production and use, Green Chem. 8 (2006) 763–780.
[5] M.C.G. Juenger, F. Winnefeld, J.L. Provis, J. Ideker, Advances in alternative cementitious binders, Cem Concr Res (in press), DOI 10.1016/j.cemconres.2010.11.012.
[6] P.V. Krivenko, Alkaline cements, in: P.V. Krivenko (Ed.), Proceedings of the First International Conference on Alkaline Cements and Concretes, VIPOL Stock Company, Kiev, Ukraine, 1994, pp. 11–129.
[7] C. Shi, P.V. Krivenko, D.M. Roy, Alkali-Activated Cements and Concretes, Taylor & Francis, Abingdon, UK, 2006.
[8] H. Xu, J.L. Provis, J.S.J. van Deventer, P.V. Krivenko, Characterization of aged slag concretes, ACI Mater. J. 105 (2) (2008) 131–139.
[9] A. Fernández-Jiménez, A. Palomo, I. Sobrados, J. Sanz, The role played by the reactive alumina content in the alkaline activation of fly ashes, Microporous Mesoporous Mater. 91 (1–3) (2006) 111–119.
[10] L. Weng, K. Sagoe-Crentsil, T. Brown, S. Song, Effects of aluminates on the formation of geopolymers, Mater. Sci. Eng. B 117 (2) (2005) 163–168.
[11] A. Hajimohammadi, J.L. Provis, J.S.J. van Deventer, The effect of alumina release rate on the mechanism of geopolymer gel formation, Chem. Mater. 22 (18) (2010) 5199–5208.
[12] P. De Silva, K. Sagoe-Crentsil, V. Sirivivatnanon, Kinetics of geopolymerization: role of Al_2O_3 and SiO_2, Cem. Concr. Res. 37 (2007) 512–518.
[13] I. García Lodeiro, A. Fernández-Jiménez, A. Palomo, D.E. Macphee, Effect of calcium additions on N–A–S–H cementitious gels, J. Am. Ceram. Soc. 93 (7) (2010) 1934–1940.
[14] C.K. Yip, G.C. Lukey, J.L. Provis, J.S.J. van Deventer, Effect of calcium silicate sources on geopolymerisation, Cem. Concr. Res. 38 (4) (2008) 554–564.
[15] P. Duxson, J.L. Provis, G.C. Lukey, S.W. Mallicoat, W.M. Kriven, J.S.J. van Deventer, Understanding the relationship between geopolymer composition, microstructure and mechanical properties, Colloids Surf. A 269 (1–3) (2005) 47–58.
[16] M. Steveson, K. Sagoe-Crentsil, Relationships between composition, structure, and strength of inorganic polymers. Part 2. Fly ash-derived inorganic polymers, J. Mater. Sci. 40 (16) (2005) 4247–4259.
[17] R.R. Lloyd, J.L. Provis, K.J. Smeaton, J.S.J. van Deventer, Spatial distribution of pores in fly ash-based inorganic polymer gels visualised by Wood's metal intrusion, Microporous Mesoporous Mater. 126 (1–2) (2009) 32–39.
[18] J.L. Provis, J.S.J. van Deventer, Geopolymerisation kinetics. 2. Reaction kinetic modelling, Chem. Eng. Sci. 62 (9) (2007) 2318–2329.
[19] A. Fernández-Jiménez, A. Palomo, Composition and microstructure of alkali activated fly ash binder: effect of the activator, Cem. Concr. Res. 35 (10) (2005) 1984–1992.
[20] D.R.M. Brew, K.J.D. MacKenzie, Geopolymer synthesis using silica fume and sodium aluminate, J. Mater. Sci. 42 (2007) 3990–3993.
[21] C.A. Rees, Ph.D. Thesis, University of Melbourne, 2007.
[22] A. Hajimohammadi, J.L. Provis, J.S.J. van Deventer, One-part geopolymer mixes from geothermal silica and sodium aluminate, Ind. Eng. Chem. Res. 47 (23) (2008) 9396–9405.
[23] W.K.W. Lee, J.S.J. van Deventer, Structural reorganisation of class F fly ash in alkaline silicate solutions, Colloids Surf. A 211 (1) (2002) 49–66.
[24] C.A. Rees, J.L. Provis, G.C. Lukey, J.S.J. van Deventer, In situ ATR-FTIR study of the early stages of fly ash geopolymer gel formation, Langmuir 23 (17) (2007) 9076–9082.
[25] C.A. Rees, J.L. Provis, G.C. Lukey, J.S.J. van Deventer, The mechanism of geopolymer gel formation investigated through seeded nucleation, Colloids Surf. A 318 (1–3) (2008) 97–105.
[26] A. Hajimohammadi, Ph.D. Thesis, University of Melbourne, 2011.
[27] R.R. Lloyd, J.L. Provis, J.S.J. van Deventer, Microscopy and microanalysis of inorganic polymer cements.1: remnant fly ash particles, J. Mater. Sci. 44 (2009) 608–619.
[28] A. Pérez-Ponce, S. Garrigues, M. de la Guardia, Determination of carbonates in waters by on-line vapor generation FTIR, Vib. Spectrosc. 16 (1) (1998) 61–67.
[29] R.M. Barrer, D.E. Mainwaring, Chemistry of soil minerals. Part XIII. Reactions of metakaolinite with single and mixed bases, J. Chem. Soc. Dalton Trans. 22 (1972) 2534–2546.
[30] J.L. Provis, Activating solution chemistry for geopolymers, in: J.L. Provis, J.S.J. van Deventer (Eds.), Geopolymers: Structures, Processing, Properties and Industrial Applications, Woodhead, Cambridge, UK, 2009, pp. 50–71.
[31] J.G. Vail, Soluble Silicates: Their Properties and Uses, Reinhold, New York, 1952.
[32] I. Halasz, M. Agarwal, R. Li, N. Miller, Vibrational spectra and dissociation of aqueous Na_2SiO_3 solutions, Catal. Lett. 117 (1–2) (2007) 34–42.
[33] J.R. Sweet, W.B. White, Study of sodium silicate glasses and liquids by infrared reflectance spectroscopy, Phys. Chem. Glasses 10 (6) (1969) 246–251.
[34] T. Fernández, G. Jose, S. Mathew, P.R. Rejikumar, N.V. Unnikrishnan, An ultra-low hydrolysis sol-gel route for titanosilicate xerogels and their characterization, J. Sol-Gel Sci. Technol. 41 (2007) 163–168.
[35] J. Osswald, K.T. Fehr, FTIR spectroscopic study on liquid silica solutions and nanoscale particle size determination, J. Mater. Sci. 41 (2006) 1335–1339.
[36] M. Criado, A. Fernández-Jiménez, A. Palomo, Alkali activation of fly ash. Effect of the SiO2/Na2O ratio. Part I: FTIR study, Microporous Mesoporous Mater. 106 (1–3) (2007) 180–191.
[37] C.A. Rees, J.L. Provis, G.C. Lukey, J.S.J. van Deventer, Attenuated total reflectance Fourier transform infrared analysis of fly ash geopolymer gel aging, Langmuir 23 (15) (2007) 8170–8179.
[38] P. Duxson, A. Fernández-Jiménez, J.L. Provis, G.C. Lukey, A. Palomo, J.S.J. van Deventer, Geopolymer technology: the current state of the art, J. Mater. Sci. 42 (9) (2007) 2917–2933.
[39] P. Duxson, J.L. Provis, Designing precursors for geopolymer cements, J. Am. Ceram. Soc. 91 (12) (2008) 3864–3869.
[40] R.R. Lloyd, J.L. Provis, J.S.J. van Deventer, Microscopy and microanalysis of inorganic polymer cements. 2: the gel binder, J. Mater. Sci. 44 (2) (2009) 620–631.
[41] J.L. Provis, G.C. Lukey, J.S.J. van Deventer, Do geopolymers actually contain nanocrystalline zeolites?—a reexamination of existing results, Chem. Mater. 17 (12) (2005) 3075–3085.